Space-Time Residual Distribution Schemes for Hyperbolic Conservation Laws

Árpád Csík[1,2,*], Mario Ricchiuto[1†], Herman Deconinck[1,‡] and Stefaan Poedts[2,§]
[1] *von Karman Institute for Fluid Dynamics, Sint-Genesius-Rode, Belgium*
[2] *Center for Plasma Astrophysics, K.U.Leuven, Belgium*

Multidimensional upwind residual distribution schemes have been developed over the last decade as a monotonicity preserving spatial discretization method for hyperbolic conservation laws on unstructured grids composed of triangles or tetrahedra. In the present paper the same schemes are proposed for the time accurate solution of hyperbolic conservation laws, based on a consistent discretization of the space-time domain. Due to the upwinding property of the schemes and an appropriate choice of the space-time mesh geometry, the solution can be decoupled on temporal slabs, allowing to construct an efficient unconditionally stable implicit time marching procedure while maintaining full consistency, monotonicity and second order accuracy both in space and time. The method has been applied to the solution of the compressible Euler equations in one and two spatial dimensions. Numerical results are shown for several test cases to demonstrate the robustness and the accuracy of the method.

Nomenclature

Vector definitions:

d: Spatial dimension of the problem (1 or 2).
$\hat{\mathbf{x}}_m$: Unit vector in the m-th spatial coordinate direction.
$\hat{\mathbf{t}}$: Unit vector in the temporal coordinate direction.
$\mathbf{Q}$: Bold characters refer to purely spatial vectors in d dimensions, with components Q_m, $m = 1, ..., d$; hence $\mathbf{Q} = Q_m \hat{\mathbf{x}}_m$, where summation over the running index m is understood.
$\vec{\mathbf{Q}}$: Bold characters with arrow refer to space-time vectors with spatial components Q_m and temporal component Q_t: $\vec{\mathbf{Q}} = \mathbf{Q} + Q_t \hat{\mathbf{t}}$.
$\mathbf{x} = x_m \hat{\mathbf{x}}_m$: Spatial position vector with Cartesian components x_m.

Flow quantities:

γ: Ratio of specific heats.
ρ: Fluid density.
$\mathbf{v} = v_m \hat{\mathbf{x}}_m$: Fluid velocity.
p: Static pressure.
$E = \frac{p}{\gamma - 1} + \frac{1}{2}\rho\, v_m v_m$: Total energy density.

Operator and matrix definitions:

$\hat{0}$: Null matrix.
$\hat{I}$: Identity matrix.
$\nabla \equiv \hat{\mathbf{x}}_m\, \partial/\partial x_m$: Spatial gradient operator.
$\vec{\nabla} \equiv \nabla + \hat{\mathbf{t}}\, \partial/\partial t$: Space-time gradient operator.

*Ph.D. candidate
†VKI Diploma Course member
‡Professor, AIAA member
§Professor, Research Associate of the F.W.O.-Vlaanderen

Introduction

OVER the last decade, a class of upwind spatial discretization technique has been developed for the numerical solution of systems of hyperbolic conservation laws on triangles (2D) and tetrahedra (3D), known as fluctuation splitting or residual distribution ($\mathcal{RD}$) schemes[3,16,17]. The method incorporates the same upwind properties which are at the basis of Godunov type finite volume methods, but carried over to a cell vertex framework with continuous solution representation as in standard Finite Element methods.

The key advantage of the $\mathcal{RD}$ method is that both a high resolution monotonic solution across discontinuities, and second order spatial accuracy in smooth *steady* flows can be achieved on arbitrary unstructured grids, based on the compact stencil of the nearest neighbors. The latter property also enables an efficient implicit and parallel implementation. Another attractive feature of the $\mathcal{RD}$ schemes is that true multidimensional information can be incorporated into the upwinding procedure, derived from the physics of the problem.

However, these schemes have been developed for the solution of steady state problems and the second order accuracy degrades to first order, when they are used in combination with the method of lines (such as Runge-Kutta schemes) for the computation of unsteady flows. Second order spatial accuracy can be recovered if a consistent mass matrix formulation is applied for the temporal derivative term (hence leading to an implicit scheme), similar to what is required in stabilized finite element methods. Another route to second order schemes in time and space is the Taylor-Galerkin ap-

simplest setting. Unfortunately, both of these methods loose the positivity properties of the underlying space discretization and lead to oscillatory solutions in the presence of discontinuities. Some cures to this problem have been investigated, *e.g.* applying a Flux Corrected Transport (FCT) technique[13]. In this approach a monotone first order solution obtained from a lumped treatment of the mass matrix (hence first order) is blended with a second order non-monotone solution obtained by a consistent mass matrix formulation[3,9,12]. A similar approach has been proposed for the explicit Lax Wendroff scheme[11,12]. However, experience has shown that a Flux Corrected Transport approach as a cure to recover monotonicity for systems lacks robustness, apart from being computationally expensive. Moreover, using FCT as a way to stabilize a characteristic based upwind scheme is very unsatisfactory from the theoretical point.

A more attractive framework might be to consider space-time methods, as *e.g.* applied in the context of stabilized finite element methods[15] or discontinuous Galerkin methods[1,8,14]. In both approaches the space-time method method is usually *discontinuous* in time (although not in[1]), in order to obtain a time marching method. Sidilkover presented space-time finite volume schemes satisfying the TVD property, also indicating possible extensions to the $\mathcal{RD}$ method[2].

More recently, Abgrall[3–5] proposed a *continuous* space-time formulation for the $\mathcal{RD}$ approach, applied to the Euler equations in two spatial dimensions. The solution representation is continuous in space-time, based on a bilinear interpolation over prismatic elements which are triangular in space and linear in time. He developed new residual distribution schemes for these elements, imposing an additional constraint of limiting the distribution to the nodes located at the forward time level. In this way, the space-time domain effectively decouples in slabs of one single row of elements per time step, thus effectively resulting in a time-marching approach with a system of equations which is implicit in the unknowns located at the forward time level of the space-time slab. In Abgrall's work, this decoupling condition, combined with a positivity requirement for the update of the solution in space-time, imposes a severe limit on the allowed time step, very similar to a CFL type condition required for explicit schemes.

In the present paper we elaborate on the same idea of a *continuous* space-time residual distribution, starting from a different philosophy. Instead of imposing the time marching (past shielding) condition directly on the distribution scheme, we use standard distribution schemes operating on piecewise linear elements developed in the past for spatial triangles and tetrahedra, but apply them to solve *unsteady* problems on space-time meshes. The intrinsic upwinding property the entire space-time domain in a sequence of temporal slabs. The slabs may consist of one or two layers of cells in the temporal direction. It turns out that the decoupling can only be obtained if the mesh satisfies certain geometric properties, *and* if the timestep for the first (or only) layer is limited by a CFL-like condition as in Abgrall's approach. However, since no decoupling condition is needed for the second layer, arbitrary CFL numbers can be applied for the combined two layer scheme, while maintaining second order accuracy and monotonicity in space-time.

The paper is organized as follows: First, standard residual distribution discretizations are briefly recalled and applied to the general discretization of the space-time domain. Then the particular space-time meshes and the decoupling condition are discussed, allowing to solve the space-time equations by marching in time on a sequence of space-time slabs. In the last section several computational results are presented for the Euler equations to demonstrate the accuracy and the robustness of the schemes. Finally some conclusions are drawn and future perspectives are given.

Space-Time Residual Distribution Discretization

Scalar Conservation Law

We consider a scalar hyperbolic conservation law in d spatial dimensions over the spatial and temporal domain $\Omega = \Omega_S \times [0, t_{max}]$ with boundary $\partial\Omega$:

$$\frac{\partial u}{\partial t} + \nabla \cdot \mathbf{G} = 0, \text{ for } \forall (\mathbf{x}, t) \in \Omega, \tag{1}$$

where $u(\mathbf{x}, t)$ is the conserved quantity and $\mathbf{G}(u)$ is the corresponding flux function. In terms of the local advection speed vector $\boldsymbol{\lambda} = \partial G_m / \partial u \, \hat{\mathbf{x}}_m$, the quasilinear form of equation (1) is written as:

$$\frac{\partial u}{\partial t} + \boldsymbol{\lambda} \cdot \nabla u = 0. \tag{2}$$

Using the space-time notations introduced before, equations (1) and (2) take the following compact form

$$\vec{\nabla} \cdot \vec{\mathbf{F}} = 0 \qquad \text{and} \qquad \vec{\boldsymbol{\lambda}} \cdot \vec{\nabla} u = 0, \tag{3}$$

where the space-time flux vector is $\vec{\mathbf{F}} = \mathbf{G} + u\,\hat{\mathbf{t}}$, and the space-time advection speed vector is $\vec{\boldsymbol{\lambda}} = \boldsymbol{\lambda} + \hat{\mathbf{t}}$.

In this paper we propose to apply standard, fully upwind residual distribution schemes[3,17] to the numerical solution of equations (3) on space-time domain Ω, discretized by triangles and tetrahedra in one and two spatial dimensions, respectively.

For a classical *continuous* (in time) stabilized Galerkin Finite Element method (such as SUPG or GLS), this would lead to a system coupling the unknowns for all of the grid points in the space-time

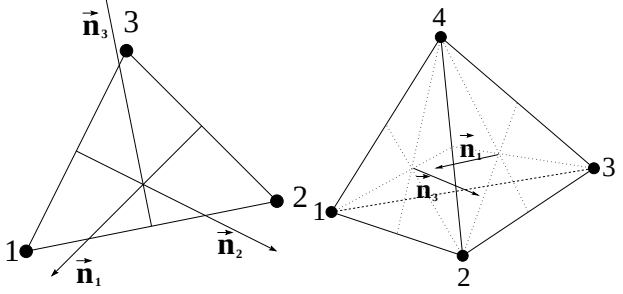

Fig. 1 Generic linear elements with inward pointing scaled normal vectors. Triangles and tetrahedra are used in one and two spatial dimensions, respectively.

domain, which is clearly unacceptable from a computational point of view. Therefore, most Finite Element approaches use a *discontinuous* formulation in time.

However, in the context of upwind $\mathcal{RD}$ methods it is possible to maintain a continuous formulation in time, *and* to decouple the space-time solution on temporal slabs with thickness Δt, such that effectively a time marching procedure is obtained. Indeed, since the temporal component of the advection speed vector $\vec{\boldsymbol{\lambda}}$ is always positive (equal to unity), the use of fully upwind $\mathcal{RD}$ schemes naturally leads to the decoupling of the solution if certain geometric conditions of the mesh are satisfied, as will be discussed below. Thus, advancing one physical step Δt in time is equivalent to the solution of a steady state problem in $d+1$ dimensions on a space-time slab $\Omega_S \times \Delta t$.

First we briefly outline the solution procedure for standard residual distribution schemes, applied to space-time meshes. For further details the reader is referred to the above references on the steady schemes. Following the standard approach, we divide the space-time domain Ω into non overlapping elements, which are triangles and tetrahedra in one and two spatial dimensions, respectively. For example, in one spatial dimension the space-time domain Ω forms a rectangle if Ω_S is fixed in time (*i.e.* non moving grids), as shown in Fig. 2. Just like in linear finite element methods, the state vector u is approximated by a continuous, piecewise linear function over Ω:

$$u(\mathbf{x},t) = \sum_{j=1}^{N} u_j w_j(\mathbf{x},t). \tag{4}$$

where N is the total number of nodes, u_j is the nodal value of the state variable u at node j and $w_j(\mathbf{x},t)$ is the corresponding piecewise linear shape function with compact support. Integration of the space-time flux divergence over element E yields the definition of the space-time cell residual:

$$\phi^E = \int_E \nabla \cdot \vec{\mathbf{F}}\, d\Omega = \int_E \vec{\boldsymbol{\lambda}} \cdot \vec{\nabla} u\, d\Omega. \tag{5}$$

tion[18], the cell residual can be written as:

$$\phi^E = \vec{\boldsymbol{\lambda}} \cdot \int_E \vec{\nabla} u\, d\Omega = \sum_{i=1}^{d+2} k_i u_i, \tag{6}$$

where $\vec{\boldsymbol{\lambda}}$ is a cell averaged space-time advection speed constructed such that

$$\vec{\boldsymbol{\lambda}} \cdot \int_E \vec{\nabla} u\, d\Omega = \oint_{\partial E} \vec{\mathbf{F}} \cdot \vec{\mathbf{n}}\, dS, \tag{7}$$

for a consistent discretization of the contour integral in the right hand side. Based on the cellwise linear approximation of u, the coefficient k_i (called upwind parameter in the following) is obtained as

$$k_i = \frac{\vec{\boldsymbol{\lambda}} \cdot \vec{\mathbf{n}}_i}{d+1}, \tag{8}$$

where $\vec{\mathbf{n}}_i = n^i_m \hat{\mathbf{x}}_m + n^i_t \hat{\mathbf{t}}$ labels the inward pointing normal vector of the face opposite to node i, scaled with the area of the face (see Fig. 1).

In the fluctuation splitting method the cell residual is distributed to the nodes of element E according to the following formula:

$$\phi^E_i = \beta^E_i \phi^E, \tag{9}$$

where the distribution function ϕ^E_i is the fraction of the total cell residual ϕ^E distributed to node i in element E, and β^E_i is the so called distribution coefficient. For consistency, we require that for a given cell E

$$\sum_{i=1}^{d+2} \phi^E_i = \phi^E \quad \text{or} \quad \sum_{i=1}^{d+2} \beta^E_i = 1,$$

where a cellwise local numbering of the nodes is used.

Different residual distribution schemes are determined by the way ϕ^E_i or β^E_i is defined. In the present context the satisfaction of appropriate multidimensional upwinding properties by the schemes is crucial, since it will ensure that no contribution of the cell residual is sent to nodes at the initial time level of the space-time slab. Multidimensional upwind $\mathcal{RD}$ schemes are defined by the condition

$$\beta^E_i = 0 \quad \text{or} \quad \phi^E_i = 0 \qquad \text{for } k_i \le 0. \tag{10}$$

Indeed, this condition expresses that residual contributions in cell E are only sent to downstream nodes, whereby a node is defined to be *downstream* if the face opposite to this node sees an *ingoing* flux (*i.e.* $k_i > 0$). In this paper we use three different schemes which satisfy this property: the optimal positive, linear, first order N scheme, the non-monotone, linear, second order LDA scheme, and the monotone, nonlinear, second order B scheme[3,6,16,17] (see appendix). Distributing

ing to equation (9) and assembling the contributions to the nodes, we arrive to the discrete form of equation (3):

$$\sum_{E,j\in E} \phi_j^E = 0 \qquad \text{for } \forall j \in [1,N]. \tag{11}$$

Equation (11) is an implicit system which in principle could involve the unknowns of all grid points in the space-time domain. However, due to the use of upwind $\mathcal{RD}$ schemes, the solution is decoupled on temporal slabs, and a time marching procedure is obtained as will be shown below. In the present paper, system (11) is solved by embedding it in a pseudo time dependent iteration procedure.

Extension to a System of Equations

We consider a system of hyperbolic conservation laws consisting of p equations in d spatial dimensions over space-time domain Ω:

$$\frac{\partial U}{\partial t} + \nabla \cdot \mathbf{G} = 0, \qquad \text{for } \forall (\mathbf{x},t) \in \Omega, \tag{12}$$

where U is the vector of conserved variables and $\mathbf{G}$ is the $p \times d$ flux vector. Equation (12) in quasilinear form reads:

$$\frac{\partial U}{\partial t} + \left(\frac{\partial G_m}{\partial U}\, \hat{\mathbf{x}}_m \right) \cdot \nabla U = 0. \tag{13}$$

Just like in the scalar case, we introduce the space-time formulation of equation (12):

$$\vec{\nabla} \cdot \vec{\mathbf{F}} = 0, \tag{14}$$

where the space-time flux vector is $\vec{\mathbf{F}} = \mathbf{G} + U\,\hat{\mathbf{t}}$. Assuming piecewise linear variation of the components of the state variable U:

$$U(\mathbf{x},t) = \sum_{j=1}^{N} U_j w_j(\mathbf{x},t), \tag{15}$$

and applying a proper conservative linearization[18], the total residual vector Φ^E in element E is written as:

$$\Phi^E = \oint_{\partial E} \vec{\mathbf{F}} \cdot \vec{n}\, dS = \left(\frac{\partial \bar{G}_m}{\partial U}\, \hat{\mathbf{x}}_m + \hat{I}\, \hat{\mathbf{t}} \right) \cdot \int_E \vec{\nabla} U\, d\Omega, \tag{16}$$

where $\partial \bar{G}_m / \partial U$ is the m-th component of the flux Jacobian taken in an averaged state of $\bar{U}$, such that conservation is satisfied according to equation (16). Introducing the following linear combination of the space-time Jacobian matrices:

$$K_i = \frac{1}{d+1} \left(\frac{\partial \bar{G}_m}{\partial U}\, n_m^i + \hat{I}\, n_t^i \right), \tag{17}$$

$$\Phi^E = \sum_{i=1}^{d+2} K_i U_i. \tag{18}$$

Since equation (12) is hyperbolic in physical time, the p eigenvalues of matrix K_i are real, and a complete set of p real linearly independent eigenvectors exists. Diagonalization of matrix K_i yields: $K_i = R_i \Lambda_i L_i$, where Λ_i is the eigenvalue matrix (diagonal matrix containing the eigenvalues in the diagonal) of K_i, the columns of R_i contain the right eigenvectors of K_i, and $L_i = (R_i)^{-1}$.

The eigenvalues and the eigenvectors of matrix K_i can be easily obtained from the eigenvalue decomposition (*i.e.* the eigenvalues and the eigenvectors) of matrix $C_i = \partial \bar{G}_m / \partial U n_m^i$. Let us rewrite equation (17) as

$$K_i = \frac{1}{d+1} (R_i \tilde{\Lambda}_i L_i + \hat{I}\, n_t^i), \tag{19}$$

where $\tilde{\Lambda}_i$ is the eigenvalue matrix of C_i. Hence, K_i can be further written as

$$K_i = \frac{1}{d+1} R_i (\tilde{\Lambda}_i + \hat{I}\, n_t^i) L_i = \frac{1}{d+1} R_i \Lambda_i L_i. \tag{20}$$

Equation (20) reflects an important property of the space-time method: Even if the original matrix C_i is singular (as occurs *e.g.* for vanishing flow speed in the case of the Euler equations), matrix K_i is still regular due to the presence of the flow independent diagonal entries. The importance of non vanishing eigenvalues in the case of quasi stagnant flow problems is clear, since the $\mathcal{RD}$ schemes require the inversion of matrices

$$\sum_{i=1}^{d+2} K_i^+ \quad \text{or} \quad \sum_{\mathrm{i}=1}^{\mathrm{d}+2} \mathrm{K}_\mathrm{i}^-, \tag{21}$$

which are singular for vanishing velocity (cfr. appendix). Although Abgrall has shown that the $\mathcal{RD}$ schemes remain well-defined in these degenerate cases, special care is required to treat the singularity, which is not necessary for the space-time approach (as will be demonstrated in the results section).

The eigenvalue matrix can be decomposed as $\Lambda_i = \Lambda_i^+ + \Lambda_i^-$, where

$$\Lambda_i^\pm = \frac{\Lambda_i \pm |\Lambda_i|}{2}. \tag{22}$$

The generalized upwind parameters $K_i^+ = R_i \Lambda_i^+ L_i$ and $K_i^- = R_i \Lambda_i^- L_i$ play an important role in the multidimensional upwind property of the system residual distribution schemes. In element E, node i does not receive any contribution from the cell residual if all of the eigenvalues of the corresponding matrix K_i are negative, *i.e.* Λ_i^+ is the null matrix (see appendix).

Φ^E. The distribution function is defined as:

$$\Phi_i^E = \beta_i^E \Phi^E, \tag{23}$$

where β_i^E is the distribution matrix. For consistency we require that

$$\sum_{i=1}^{d+2} \Phi_i^E = \Phi^E \quad \text{or} \quad \sum_{i=1}^{d+2} \beta_i^E = \hat{I}. \tag{24}$$

The definition of Φ_i^E for the system version of the N, LDA and B-scheme is given in the appendix.

Finally, assembling the contributions from the surrounding elements, the discretization of equation (12) is given by

$$\sum_{E, j \in E} \Phi_j^E = 0, \qquad \text{for } \forall j \in [1, N]. \tag{25}$$

Remark on the Conservative Linearization

If the spatial flux function $\mathbf{G}$ is a non linear function of u (scalar) resp. U (system), then the same rules apply for the conservative linearization as in the steady case. For example, if $\mathbf{G}$ and u resp. U can be written as a quadratic function of a certain Roe parameter variable z resp. Z, then the Struijs-Deconinck-Roe linearization[18] can be used to achieve full conservation of the space time fluxes.

Geometry of the Space-Time Grid

In order to design an efficient time marching procedure, the full space-time solution of the problem has to be decoupled into temporal slabs. It turns out, that upwind $\mathcal{RD}$ schemes operating on properly constructed space-time geometries naturally lead to such a temporal decoupling of the solution. In this paper we propose to use a space-time mesh containing three levels of nodes and two layers of elements in the temporal direction, see[7] for some details about the single layer version of the approach. The first, second, and third levels of nodes have temporal coordinates t_n, $t_{n+1/2}$, and t_{n+1}, and will be called respectively *past*, *intermediate* and *future* time level. The space-time solution is decoupled if no residual contribution is sent from the cells of the two layers to the nodes located at the *past* level ($t = t_n$).

Two layers appear to be the minimum necessary to allow for a scheme with unconditionally stable implicit time stepping. The time step $\Delta t_1 = t_{n+1/2} - t_n$ is limited by a severe CFL-like condition similar to explicit schemes in order to decouple the solution in the first layer of elements (see below). However, in the second layer an arbitrary time step $\Delta t_2 = t_{n+1} - t_{n+1/2}$ can be taken. The effective CFL number for the whole temporal slab is controlled by the ratio Q of the time steps over the two layers:

$$Q = \Delta t_2 / \Delta t_1.$$

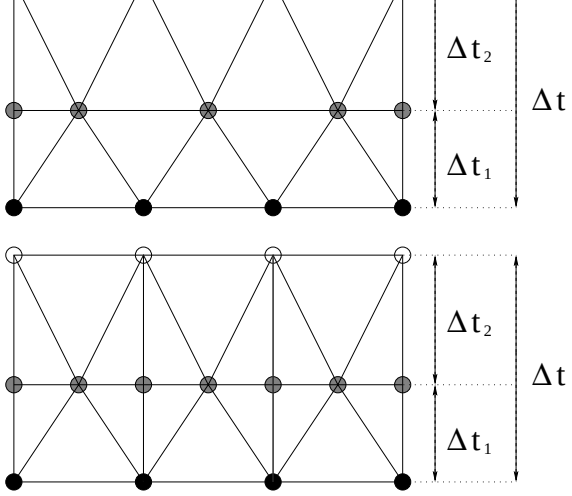

Fig. 2 Valid configurations of the space-time mesh in 1D. Nodes at levels n, $n+1/2$ and $n+1$ are labelled by black, gray and empty circles, respectively.

One Spatial Dimension

Fig. 2 shows two valid configurations of the space-time mesh. Both configurations require some nodes in the intermediate level which are staggered in space, located at the midpoints of the segments on the past level as will be shown below. The top configuration is optimal in terms of computational cost and will be used in all computational experiments. The second configuration is also useful, as it allows more easily for a generalization in two space dimensions. In both configurations, the second layer of triangles is obtained from the first layer by mirroring it to the $t = t_{n+1/2}$ line. Then the temporal width of the mirrored layer is stretched according to the ratio Q. The first layer of the space-time mesh contains two types of triangles, E1 and E2 (see Fig. 3). Triangles of type E1 have two past nodes and one intermediate node, while triangles of type E2 have one past node and two intermediate nodes.

Decoupling condition for a scalar conservation law

In order to decouple the solution and allow time marching, no contribution of the residual must be sent to the past level from the triangles of the first layer, *i.e.* the upwind parameter k_i must be non positive for all of the past nodes i according to condition (10).

For triangles of the E2 type the value of k_i for the unique past node is $k_i = -\Delta x/2 < 0$, therefore this node never receive a residual contribution from these elements.

Let us consider a triangle of type E1 as shown in Fig. 3. Using local numbering of the nodes, the inward scaled normal vectors are $\vec{\mathbf{n}}_1 = (-\Delta t_1, -\Delta x/2)$, $\vec{\mathbf{n}}_2 = (\Delta t_1, -\Delta x/2)$, and $\vec{\mathbf{n}}_3 = (0, \Delta x)$. The corresponding upwind parameters for the nodes at the past level are therefore $k_1 = -\bar{\lambda}\Delta t_1/2 - \Delta x/4$ and $k_2 = \bar{\lambda}\Delta t_1/2 - \Delta x/4$, where $\bar{\lambda} = \partial \bar{F}_x / \partial u$ is the spatial

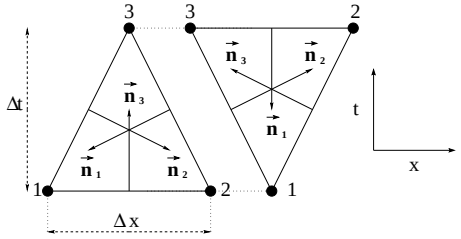

Fig. 3 Basic triangular elements in the first layer of the space-time mesh in one spatial dimension.

component of the linearized advection speed vector. Imposing that both k_1 and k_2 must be non positive leads to the following local time step restriction:

$$CFL_1 = \left(\frac{\Delta t_1 \left| \bar{\lambda} \right|}{\Delta x} \right)_E \leq \frac{1}{2} \quad \forall E \in E_1 \tag{26}$$

Equation (26) is called the *local past shield* (LPS) condition, since its satisfaction guarantees that the past nodes are locally protected from any artificial propagation of information from the future due to element E1. The global timestep Δt_1 for the first layer is obtained from

$$\Delta t_1 \leq \min_{\forall E \in E_1} \left(\frac{\Delta x}{2 \left| \bar{\lambda} \right|} \right)_E . \tag{27}$$

Clearly, the intermediate nodes can be coupled with the past and future nodes if the two layers are solved in one implicit system. Therefore, no condition is required for the time step Δt_2 of the second layer, which enables to take large physical time steps. Using the ratio Q, the total time step can be written as

$$\Delta t = \Delta t_1 + \Delta t_2 = (Q+1) \min_{\forall E \in E1} \left(\frac{\Delta x}{\left| \bar{\lambda} \right|} \right)_E CFL_1, \tag{28}$$

where $CFL_1 \leq 1/2$. This leads to the following effective CFL number:

$$CFL = \frac{\Delta t \left| \bar{\lambda} \right|}{\Delta x} = (Q+1) CFL_1. \tag{29}$$

Equation (29) shows that in case of large value of the time step ratio Q, the schemes can operate at high CFL numbers, while maintaining the unconditional linear stability and positivity properties of the underlying $\mathcal{RD}$ schemes. This property is extremely useful when the spatial mesh contains highly refined regions. Due to the unconditional stability of the schemes, the global time step is not restricted by the presence of very small elements, which is the case when an explicit type CFL condition must be satisfied.

The method extends trivially to a hyperbolic system of equations by applying the *system* version of the upwind $\mathcal{RD}$ schemes (see appendix). These schemes do not distribute any residual to a node if all the eigenvalues of the corresponding matrix K_i are non positive ($\Lambda_i^+ = \hat{0}$), for nodes i belonging to the past level. For the Euler equations in one space dimension, this leads to the following LPS condition:

$$CFL_1 = \left(\frac{\Delta t_1 (|\bar{v}| + \bar{c})}{\Delta x} \right)_E \leq \frac{1}{2} \quad \forall E \in E_1, \tag{30}$$

where $\bar{v}$ and $\bar{c}$ are the averaged flow speed and sound speed, respectively. The global condition follows as in the scalar case.

Geometrical conditions on the space-time mesh in 1D

Consider the case of a general space-time triangle of type E1 as shown in Fig. 4. The parameter α defines the spatial location of the node at the intermediate time level. For $|\alpha| > \frac{1}{2}$, one obtains an obtuse triangle (*i.e.* the projection of node 3 falls outside the edge located at level n), while $\alpha = 0$ corresponds to the symmetric cases discussed before (Fig. 2). The face normals are given by

$$\vec{\mathbf{n}}_1 = (-\Delta t_1, -(\tfrac{1}{2} - \alpha)\Delta x), \tag{31}$$

$$\vec{\mathbf{n}}_2 = (\Delta t_1, -(\tfrac{1}{2} + \alpha)\Delta x), \tag{32}$$

$$\vec{\mathbf{n}}_3 = (0, \Delta x). \tag{33}$$

Expressing again the decoupling condition for nodes 1 and 2, one observes that no positive solution for Δt_1 exists for $|\alpha| > \frac{1}{2}$, thus excluding obtuse triangles of type E1 in the first layer. For $|\alpha| < \frac{1}{2}$ the time step limitation on the first layer is

$$CFL_1 = \frac{\Delta t_1 \left| \bar{\lambda} \right|}{\Delta x} \leq \frac{1}{2} - |\alpha|. \tag{34}$$

One observes that the CFL condition on the first layer becomes more and more severe as $|\alpha|$ approaches $\frac{1}{2}$, giving the unacceptable limit solution $\Delta t_1 = 0$ for the Cartesian grid case shown in Fig. 5. Hence, the value $\alpha = 0$ used for both configurations of Fig. 2 is optimal in terms of maximal allowable timestep for arbitrary sign of the characteristic speed.

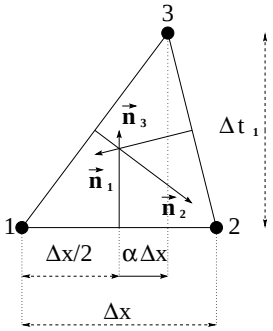

Fig. 4 General triangle of type E1 in the first layer of a space-time mesh.

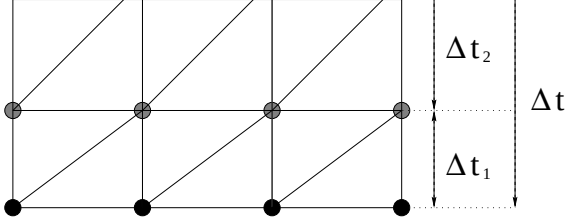

Fig. 5 Unacceptable Cartesian space-time mesh

Space-time Mesh in Two Spatial Dimensions

As in 1D, different mesh configurations are possible. Starting from a given arbitrary triangulation in space, the simplest (but not the most economic) choice is probably the following generalization (see Fig. 6) of the 1D configuration shown at the bottom of Fig. 2. The first layer of elements is built from three types of tetrahedra as shown in Fig. 7. Type E1 has three past nodes situated at level n, and one node at the intermediate level $n+\frac{1}{2}$. The spatial position of the intermediate node is at the centroid of the triangles of the original 2D mesh. Type E2 has two past and two intermediate nodes. Finally, type E3 has one past node and three intermediate nodes. The second layer of elements is obtained from the first layer by mirroring to the $t = t_{n+1/2}$ plane, and stretching the temporal width of the mirrored layer according to the ratio Q, as in the 1D case.

Decoupling condition for the scalar case

Consider the generic tetrahedra E1, E2, and E3 of the first layer. It is straightforward to show that for elements of type E3 no contribution of the residual is sent to the unique past node. Expressing the decoupling condition for generic tetrahedron E1 for the 3

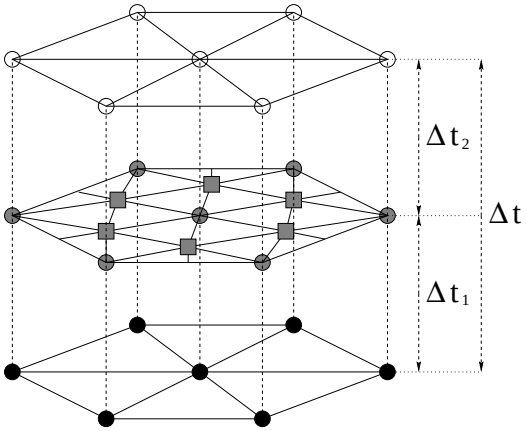

Fig. 6 Positioning of the nodes in the space-time mesh in 2D. Nodes at levels n, $n+1/2$ and $n+1$ are respectively labelled by black, gray and empty circles. Squares indicate intermediate nodes positioned in the centroid of the triangles of the level n spatial mesh.

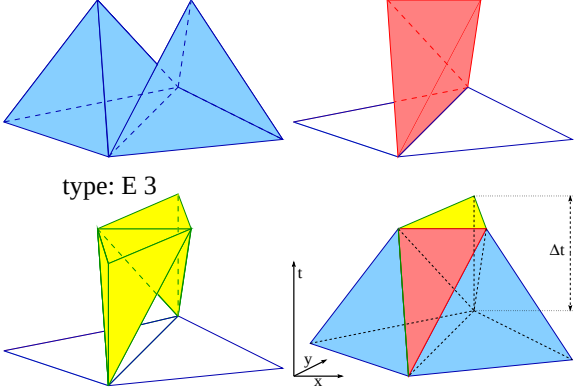

Fig. 7 Three types of basic tetrahedra used to build the first layer of the space-time mesh in two space dimensions, and schematic view of the mesh.

past nodes leads to (using the notation of Fig. 8):

$$CFL_1^{E1} = \max_{j=1,2,3} \left(\frac{k_j^+ \, \Delta t}{S_j} \right)_{E1} < 1, \qquad (35)$$

where $S_j = n_j^t$ is the temporal component of $\vec{\mathbf{n}}_\mathbf{j}$, i.e. the area of the face opposite to vertex j in the tetrahedron, projected on the level n plane. For the present configuration where node 4 is located in the centroid of the base triangle, this area is easily calculated as $1/3$ of the area of the base triangle. On the other hand, $k_j^+ = \max(0, k_j)$, where

$$k_j = \frac{\bar{\boldsymbol{\lambda}} \cdot \mathbf{n}_j^{123}}{2},$$

which is the inflow parameter corresponding to vertex j of the base triangle (i.e. $\mathbf{n}_j^{123}$ is scaled with the length of the edge opposite to j). A similar analysis for the past nodes 1 and 2 of the generic tetrahedron of type E2 leads to the condition

$$CFL_1^{E2} = \max_{j=1,2} \left(\frac{k_j^+ \, \Delta t}{S_j} \right)_{E2} < 1, \qquad (36)$$

where $S_j = n_j^t$ is defined as before (computed to be equal to the area of the face opposite to node j in the tetrahedron, projected on the level n plane) and

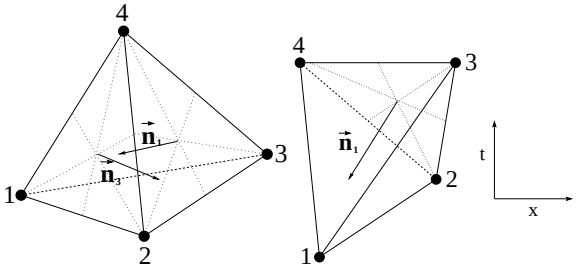

Fig. 8 Elementary tetrahedra of types E1 (left) and E2 (right), see also Fig. 7.

triangle Δ^{j34}. Equations (35) and (36) have to be simultaneously satisfied in all of the tetrahedra of types E1 resp. E2, giving the global time step limitation for the first layer

$$\Delta t_1 = CFL_1 \min \left(\min_{E\in E_1} \left(\frac{1}{\max\limits_{j=1,2,3} \frac{k_j^+}{S_j}}\right), \min_{E\in E_2} \left(\frac{1}{\max\limits_{j=1,2} \frac{k_j^+}{S_j}}\right) \right) \tag{37}$$

with $CFL_1 \leq 1$.

Just like in the 1D case, there is no restriction on the time step of the second layer. By increasing the value of the time step ratio Q, arbitrarily large global time steps can be taken according to

$$\Delta t = (Q+1)\Delta t_1 \tag{38}$$

with an effective CFL corresponding to

$$CFL = (Q+1)CFL_1 \tag{39}$$

Decoupling condition for the system case

The analysis extends again trivially to the system case. The scalar inflow parameter k_j^+ in equations (35) and (36) is replaced by the largest eigenvalue of the space Jacobians K_i^+.

Geometrical conditions on the space-time mesh in 2D

Considering the case of a general space-time tetrahedron of type E1, one obtains similar results as in the 1D case. The area's S_j in eq. (35) are now proportional to the area coordinates of node 4 in the base triangle (equal to 1/3 if node 4 coincides with the centroid). Hence, at least one of the S_j becomes negative if the projection of node 4 on the level n plane falls outside the base triangle, and no positive solution for Δt_1 exists in this case. Similarly, if node 4 approaches the boundary opposite to node j, S_j approaches zero and the allowable time step approaches zero. Hence, for an arbitrary convection speed vector, the location of node 4 in the gravity center leads to the largest allowable time-step.

For tetrahedra of type E2, one arrives at the condition that the projection of the straight line through edge 3-4 on the level n plane has to cut the segment 1-2 in between the nodes 1 and 2. This condition is always satisfied if no obtuse triangles exist in the spatial mesh, but it could be violated for severely distorted space meshes with obtuse triangles.

Numerical Results

The space time residual distribution method discussed so far has been applied for the solution of the 1D and 2D Euler equations governing inviscid compressible flows. The state vector U and the flux $\mathbf{G}$ are

$$U = \begin{pmatrix} \rho \\ \rho \mathbf{v} \\ E \end{pmatrix} \text{ and } \mathbf{G} = \begin{pmatrix} \rho \mathbf{v} \\ \rho \mathbf{v}\mathbf{v} + \hat{I}p \\ (E+p)\mathbf{v} \end{pmatrix}, \tag{40}$$

respectively, where the notation of the flow variables has been given in the nomenclature.

Verification of the Order of Accuracy

The order of accuracy for the space-time method has been verified in[7] for smooth testcases in one space dimension with known analytic solution. The observed order of accuracy is summarized in table 1. Results indicate that the measured accuracy in space time preserves the formal accuracy of the $\mathcal{RD}$ schemes[3].

Distribution Scheme:	N	LDA	B
Steady nozzle (density):	1.00	2.01	2.14
Unsteady advection:	0.97	2.00	1.66

Table 1. Measured order of accuracy of the N, LDA and B schemes.

1D Shu-Osher Riemann Problem

We perform the computation of a test case proposed by Shu and Osher[19], corresponding to the propagation of a Mach 3 shock into a uniform domain superimposed by a sinusoidal density perturbation. The initial state is given by $\rho_L = 3.857143$, $v_{x,L} = 2.629367$, $p = 10.33333$ for $x \leq -4$ and $\rho_R = 1 + 0.2sin(5x)$, $v_{x,R} = 0$, $p_R = 1$ for $x > -4$. In the computation we use $Q = 2$ and $CFL = 1.49$. The solution computed by the second order non linear B-scheme at $t = 1.8$ is shown on the left of Fig. 9 and 10 for 401 and 801 spatial nodes, respectively. The solid line corresponds to a solution on 1601 spatial nodes. For comparison we also show computational results published by Shu and Osher[19]: The right of Fig. 9 and 10 show the reference result for a third order ENO scheme on 400 points and a second order MUSCL type finite volume scheme on 800 points, respectively. The comparisons indicate that the second order space-time $\mathcal{RD}$ B-scheme matches surprisingly well with the third order ENO scheme on this test case, although the third order ENO-scheme is undoubtly more accurate. However, the second order space-time $\mathcal{RD}$ scheme is definitely more accurate than the second order MUSCL-scheme used by Shu and Osher[19] for their comparison.

2D Sound Wave Interaction

This test case concerns the propagation and interaction of linear sound waves in a two-dimensional stagnant flow. As initial state, two exponentially decaying axisymmetric pressure perturbations with a maximum amplitude of $\delta p = 0.1$ are superposed onto a stagnant background with $\rho = 140$, $\vec{\mathbf{v}} = 0$, and $p = 100$. In the solution of this problem the pressure perturbations are

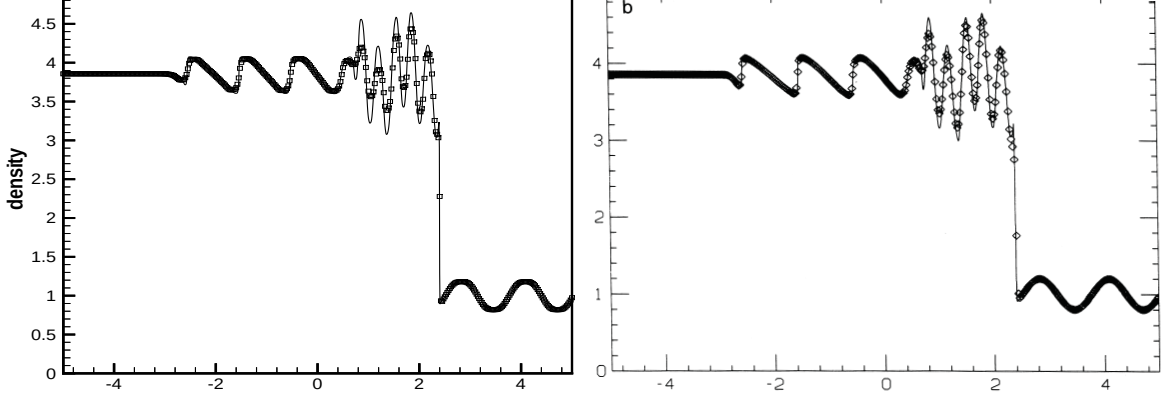

Fig. 9 Shu-Osher test case at $t = 1.8$. Left: Solution for the second order nonlinear B-scheme on 401 nodes in space. Right: Reference solution computed by a third order ENO scheme on 400 points[19].

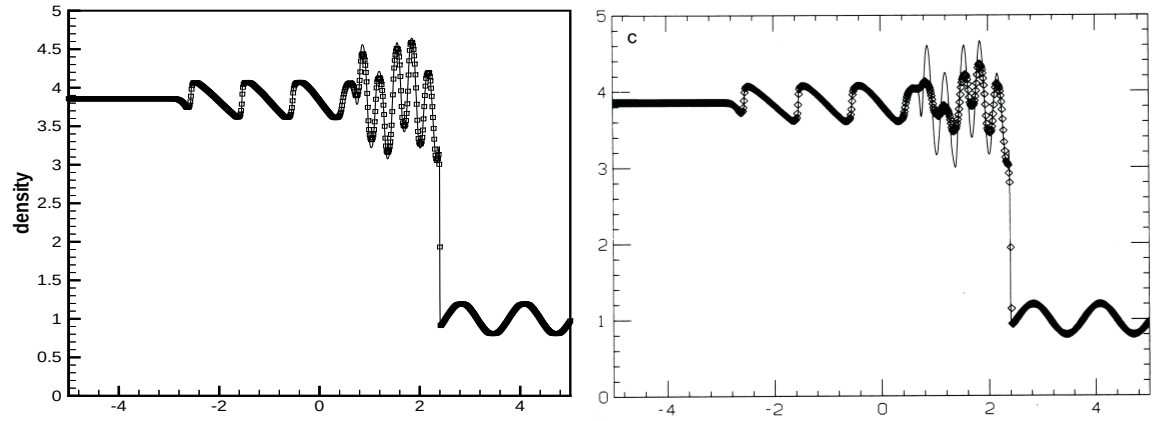

Fig. 10 Shu-Osher test case at $t = 1.8$. Left: Solution for the second order nonlinear B-scheme on 801 nodes in space. Right: Solution for a second order MUSCL TVD Finite Volume scheme on 800 points[19].

propagated in the radial direction in the form of linear sound waves, with the speed of sound. In Fig. 11 we show a series of snapshots at different time steps, computed by the second order linear LDA-scheme on a mesh containing 101×101 points in space. On the last two plots the interference of the two waves can be observed. This testcase illustrates the robustness of the method for quasi-static problems without the need of any special treatment.

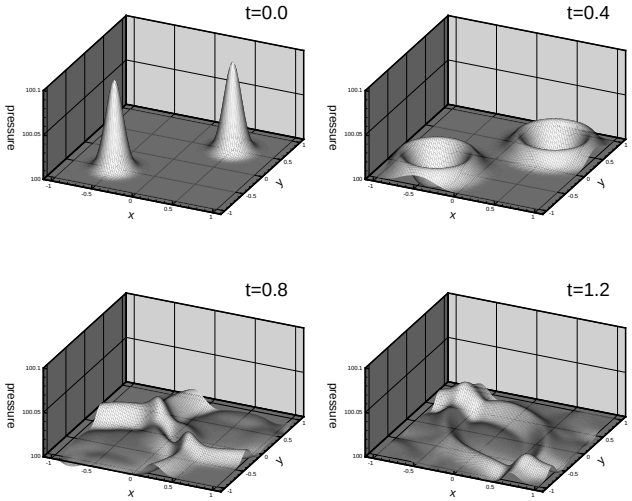

Fig. 11 Interaction of linear sound waves. Four snapshots of the pressure surface for a mesh with 101 X 101 nodes. Computation made with the second order linear LDA-scheme.

2D Riemann Problem

To further validate the method in two spatial dimensions we propose a truely 2D Riemann problem. At $t = 0$ a squared shaped $[3.6 \times 3.6]$ uniform domain with $\rho_1 = 3$, $\mathbf{v_1} = 0$ and $p_1 = 3$ is embedded into an infinite uniform domain with $\rho_2 = 1$, $\mathbf{v}_2 = 0$ and $p_2 = 1$. For symmetry reasons it is sufficient to compute the solution over one quarter of the full domain. The solution is computed at $t = 0.4$ on a structured triangulation of the 2D spatial domain containing 101×101 points in space ($\Delta x = \Delta y = 0.02$).

The density and pressure surfaces are shown in Fig. 12 and 13 for the first order N and the second order

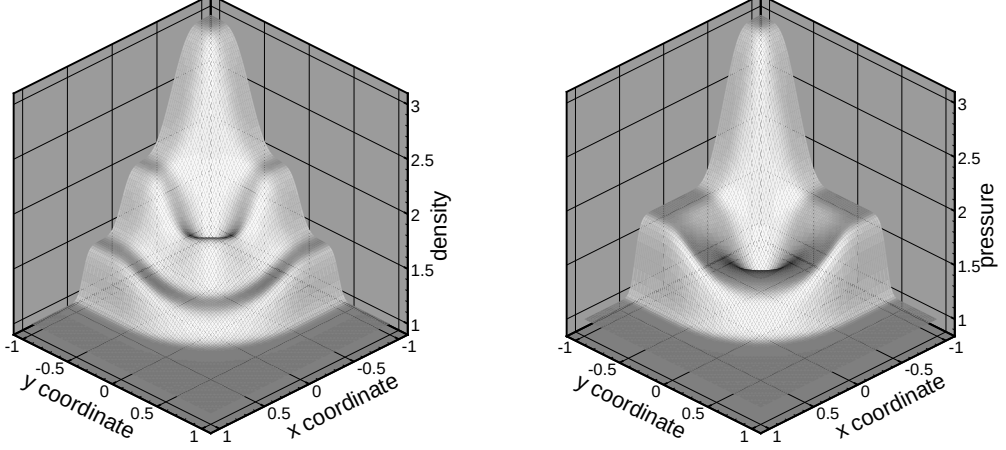

Fig. 12 2D Riemann problem computed by the first order linear N scheme at t=0.4.

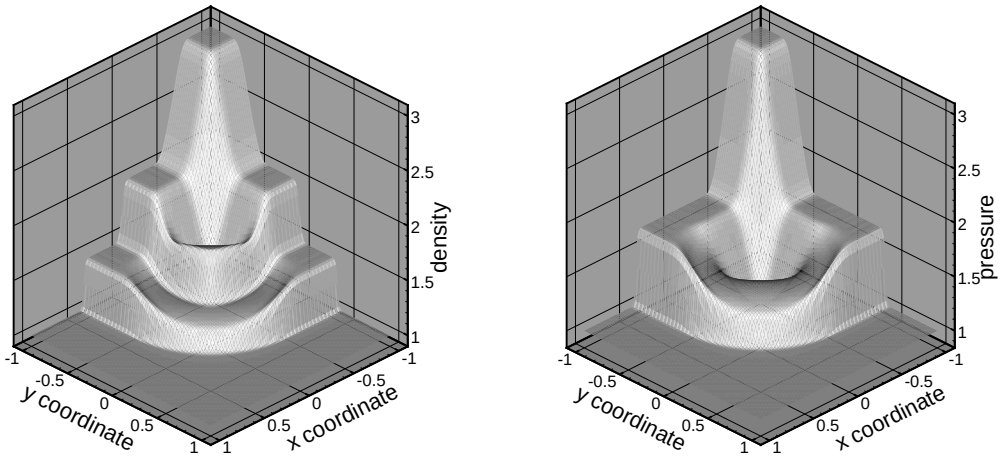

Fig. 13 2D Riemann problem computed by the second order nonlinear B scheme at t=0.4.

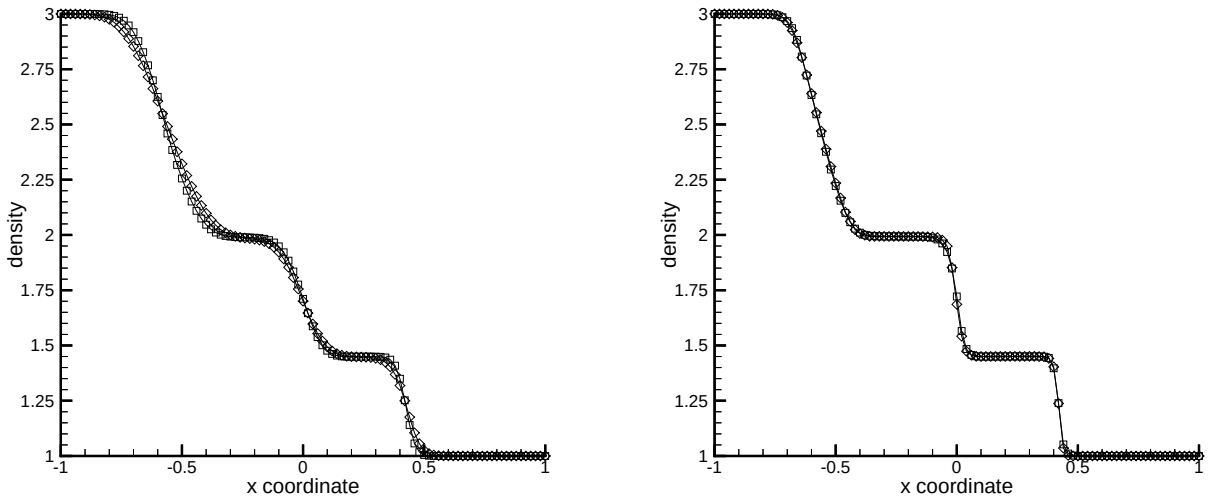

Fig. 14 Riemann solution at $t = 0.4$. Profile of density. Squares: True 1D solution. Diamonds: 2D solution along the x-axis. The mesh size is $\Delta x = 0.02$. Left: Computations made by the first order linear N-scheme. Right: Computations made by the second order non linear B-scheme.

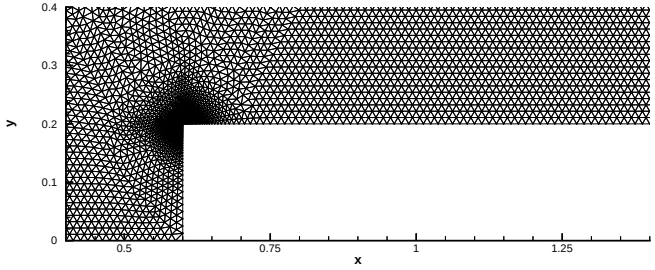

Fig. 15 Mach 3 flow over a forward facing step. Part of the unstructured grid close to the corner of the step

B schemes, respectively. The shock, shear and the expansion are well resolved in both spatial directions. Since at $t = 0.4$ the corner effect of the 2D Riemann problem has not reached the boundaries of the computational domain, the solution on the coordinate axes is identical to the solution of the 1D Riemann problem with the same initial data. In Fig. 14 we show the density computed by the 1D scheme (on a mesh with the same spacing) and the cut along the x-axis of the 2D computation for both the N and B schemes. We observe that the 2D solution on the x-axis accurately matches the true 1D solution in the case of the second order B-scheme. For the N-scheme, the 2D solution shows some additional spatial diffusion caused by the triangulation of the space domain.

Mach 3 Wind Tunnel with a Forward Facing Step

To illustrate the benefit of the unconditionally stable implicit $\mathcal{RD}$ schemes, we compute the testcase problem of a uniform triangulation of the domain with average size of the triangles given by $h = 1/80$, except for the corner of the step, where a severe local refinement was used, as shown in Fig. 15. This refinement is necessary to limit the numerical entropy production at the corner, see also[8] for more details. In total the spatial mesh has 38,740 triangles and 19,715 nodes.

The computation is made with the second order nonlinear B-scheme using the double layer approach on space-time tetrahedra. The global timestep is chosen such that $CFL \approx 1$ for the triangles in the uniform region. However, in the corner region this amounts to a local value of $CFL \approx 12$, due to the small size of the cells in this area. This clearly shows the benefit of an unconditionally stable implicit scheme, even for unsteady computations.

Isolines of the density at different instances in time are presented in Fig. 16 and 17, and compared with the solution of Collella and Woodward[20]. This reference solution is computed with a third order PPM method on a uniform mesh with square cells of size $h = 1/80$ (note that in the reference computation entropy was fixed at the corner in order to avoid the artificial entropy generation).

Flow in a channel with a bump

We compute a transonic flow in a channel[21] with a sinusoidal bump at the bottom, with an inlet Mach number $M_\infty = 0.675$. As inlet conditions we impose flow angle ($\alpha = 0$), together with total temperature and total pressure (computed relative to the inlet Mach number). At the outlet we impose an oscillating static pressure, given by $p_{out} = p_0 + p_1 \sin \omega t$, with

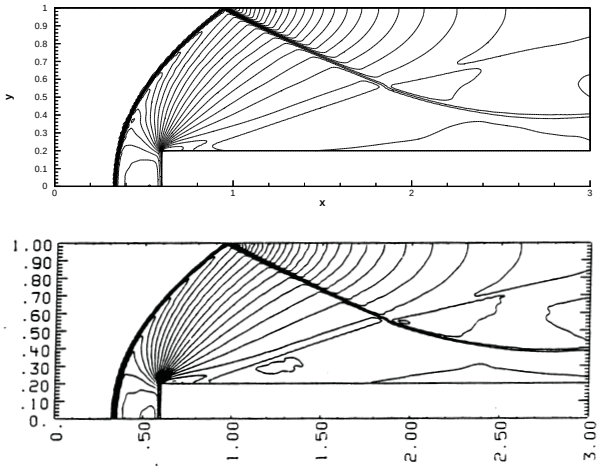

Fig. 16 Mach 3 flow over a forward facing step: Density iso-lines at $t = 1.0$. Top: nonlinear second order space-time B-scheme. Bottom: Reference solution: third order PPM scheme on Cartesian mesh[20].

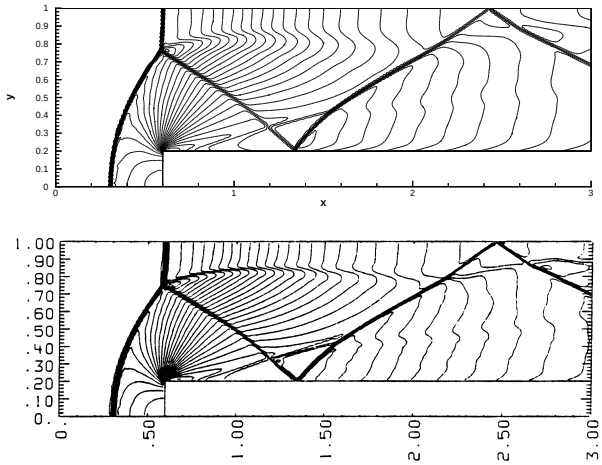

Fig. 17 Mach 3 flow over a forward facing step: Density iso-lines at $t = 4.0$. Top: nonlinear second order space-time B-scheme. Bottom: Reference solution: third order PPM scheme on Cartesian mesh[20].

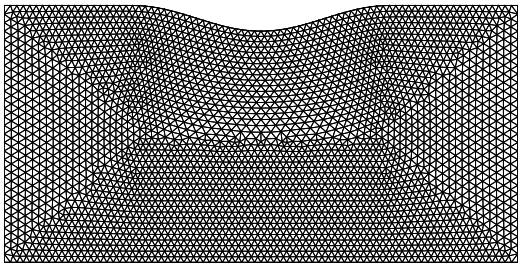

Fig. 18 The mesh used for the computation of the flow in a channel with a bump. It contains 3,162 nodes and 6,102 elements.

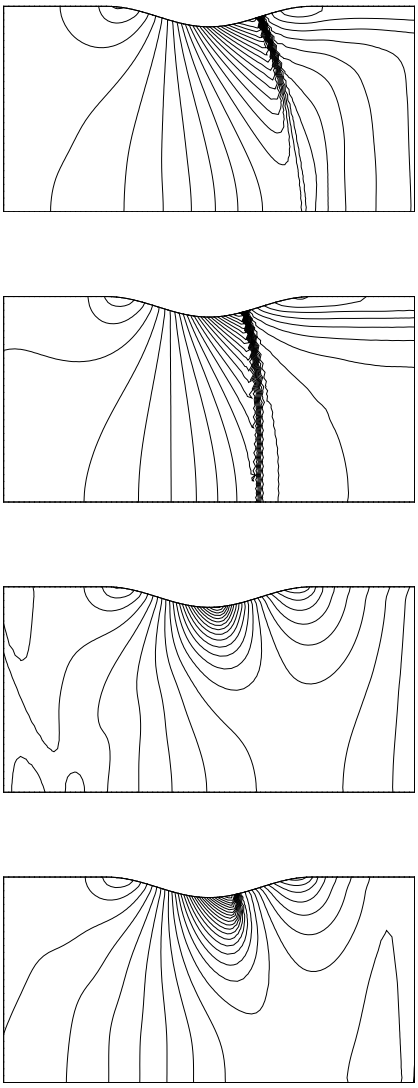

Fig. 19 Transonic flow in a channel with oscillating back pressure. Mach number contours (from top to bottom) at $t = 2\pi/\omega$, $t = 2.5\pi/\omega$, $t = 2.75\pi/\omega$ and $t = 3.5\pi/\omega$.

The spatial grid containing 3,162 nodes and 6,102 elements is shown on Fig. 18. The time evolution of the Mach number contours of the solution computed with the nonlinear B-scheme is shown in Fig. 19, for $t = 2\pi/\omega$, $t = 2.5\pi/\omega$, $t = 2.75\pi/\omega$ and $t = 3.5\pi/\omega$. At $t = 2.5\pi/\omega$ the shock has reached the bottom wall and is moving backwards. At $t = 2.75\pi/\omega$ the shock has disappeared and the outlet pressure is increasing. At $t = 3.5\pi/\omega$ the shock reappears again on the top wall. After a full period of the outlet pressure evolution at $t = 4\pi/\omega$, the solution is again identical to the one shown in Fig. 19 (top).

Conclusions

Previously developed multidimensional upwind residual distribution schemes on simplex elements have been extended to space-time domains for solving unsteady hyperbolic systems. Thus, positivity and linearity preservation properties of the original schemes are carried over to the full space-time solution, *i.e.* the linearity preserving schemes retain second order accuracy in smooth flows and the positive schemes produce oscillation free solution across discontinuities both in space and time.

Due to the intrinsic upwinding properties of the standard $\mathcal{RD}$ schemes, the space-time solution is obtained as a sequence of implicit solutions on temporal slabs consisting of two layers of elements. In the first layer an explicit type CFL condition of order one is required, but in the second layer an arbitrary CFL number can be taken.

The space time $\mathcal{RD}$ schemes have been applied to the time accurate solution of different scalar conservation laws and to the system of Euler equations both in one and two spatial dimensions. Numerical results in one space dimension demonstrate that the presented second order space-time $\mathcal{RD}$ schemes are definitely more accurate than standard second order TVD finite volume schemes, e.g. combined with a higher order Runge Kutta time integrator, and even compare favorably with a third order ENO scheme. Results in 2D have been compared favorably with a third order PPM scheme on Cartesian grids.

The key advantage of the present $\mathcal{RD}$ schemes over the bilinear schemes proposed by Abgrall is that they allow an unconditionally stable implicit time stepping, while in the schemes of Abgrall an explicit type CFL condition has to be satisfied in order to maintain positivity. Also, our $\mathcal{RD}$ schemes are not sensitive to the presence of static backgrounds, since a non vanishing eigenvalue regularizes the Jacobians for that case. This feature has its advantage at the level of coding, since no particular treatment is needed for zero flow speeds. However, the schemes proposed by Abgrall seem to be less dissipative for shear flows than our $\mathcal{RD}$ schemes.

Future work on the space-time $\mathcal{RD}$ approach is

For these problems the method offers a great potential, since the space mesh can evolve arbitrarily in time, e.g. allowing changes in topology and number of grid points without any need for interpolation data on the new mesh. Also the efficient solution of the implicit system on the space-time slab (not discussed in the present paper), needs further investigation.

The most important challenge for the future is the extension in three space dimensions. No attempt in this direction has been made yet, although the underlying schemes trivially generalize to four-dimensional hyper-tetrahedra. The biggest problem to handle is probably the construction of the four-dimensional space-time slabs satisfying the upwinding conditions, and the computational cost involved to solve the implicit systems. In this respect, the $\mathcal{RD}$ schemes proposed by Abgrall generalize much easier, since the construction of the space-time slab is immediate.

Appendix

Definition of Some Distribution Functions

Scalar N scheme: $\phi_i^N = k_i^+(u_i - u_{in})$, where

$$u_{in} = \frac{\sum_{i=1}^{d+2} k_i^- u_i}{\sum_{i=1}^{d+2} k_i^-}.$$

Scalar LDA scheme: $\phi_i^{LDA} = \beta_i^{LDA}\phi^T$,where

$$\beta_i^{LDA} = \frac{k_i^+}{\sum_{i=1}^{d+2} k_i^+}.$$

Scalar B scheme: $\phi_i^B = \theta\phi_i^N + (1-\theta)\phi_i^{LDA}$, where

$$\theta = \frac{\phi^T}{\sum_{i=1}^{d+2} |\phi_i^N|}.$$

System N scheme: $\Phi_i^N = K_i^+(U_i - U_{in})$, where

$$u_{in} = \left(\sum_{i=1}^{d+2} K_i^-\right)^{-1} \sum_{i=1}^{d+2} K_i^- U_i.$$

System LDA scheme: $\Phi_i^{LDA} = \beta_i^{LDA}\Phi^T$, where

$$\beta_i^{LDA} = \left(\sum_{i=1}^{d+2} K_i^+\right)^{-1} K_i^+.$$

System B scheme: $\Phi_i^B = \Theta\Phi_i^N + (1-\Theta)\Phi_i^{LDA}$, where

$$\Theta_{j,j} = \frac{\Phi_j^T}{\sum_{i=1}^{d+2} |\Phi_{i,j}^N|}.$$

[1] R.B. Lowrie, P.L. Roe and B. van Leer, Space-time methods for hyperbolic conservation laws, in *Barriers and Challenges in Computational Fluid Dynamics*, Kluwer Academic Publishers, pp: 79-98, 1998

[2] D. Sidilkover, A New Time-space Accurate Scheme for Hyperbolic Problems I: Quasi-explicit Case, ICASE Report No. 98-25, 1998

[3] H. Deconinck, K. Sermeus and R. Abgrall, Status of Multidimensional Upwind Residual Distribution Schemes and Applications in Aeronautics, *AIAA-CP 2000-2328*, 2000

[4] R. Abgrall and M. Mezine, A consistent upwind residual scheme for unsteady advection problems, presented at the AMIF conference, Tuscany, Italy, 2000

[5] R. Abgrall, In Schémas distribués en mécanique des fluides et applications, Proc. of Short Course, CEA-EDF-INRIA, 2000

[6] Á. Csík, H. Deconinck and S. Poedts, Monotone Residual Distribution Schemes for the Ideal 2D MHD on Unstructured Grids, *AIAA-CP 99-3325*, 644-656, 1999

[7] Á. Csík and H. Deconinck, Space Time Residual Distribution Schemes for Hyperbolic Conservation Laws on Unstructured Linear Finite Elements, in Proc. ICFD conf., Oxford, 2001

[8] B. Cockburn, Discontinuous Galerkin Methods for Convection-Dominated Problems, in *High-Order Methods for Computational Physics*, editors T.J.Barth and H.Deconinck, pp:69-224, 1999

[9] A. Ferrante and H. Deconinck, Solution of the Unsteady Euler equations using Residual Distribution and flux corrected transport, PR1997-08, Von Karman Institute, 1997

[10] Maerz and G. Degrez, Improving time accuracy of residual distribution schemes, PR1996-17, von Karman Institute, 1996

[11] M. Ricchiuto and H. Deconinck Time accurate solution of hyperbolic partial differential equations using FCT and residual distribution, SR1999-33, von Karman Institute, 1999

[12] M.E. Hubbard and P.L. Roe, Compact high-resolution algorithms for time-dependent advection on unstructured grids, International Journal for Numerical Methods in Fluids, Vol. 33, No. 5, pp: 711-736, 2000

[13] R. Lohner, K. Morgan J. Peraire and M. Vahdati, Finite element flux-corrected transport for the Euler and Navier-Stokes equations, International Journal for Numerical Methods in Fluids, Vol. 7, pp: 1093-1109, 1997

[14] Peter Hansbo, The characteristic streamline diffusion method for convection-diffusion problems, Computer Methods in Applied Mech. and Eng., Vol. 96, pp: 239-253, 1992

[15] Claes Johnson, The streamline diffusion finite element method for compressible and incompressible flow, Lecture Series: Computational Fluid Dynamics, von Karman Institute, 1990

[16] H. Paillere, H. Deconinck and P.L. Roe, Conservative upwind residual distribution schemes based on the steady characteristics of the Euler equations, *AIAA-CP 95-1700*, pp: 592-605, 1995

[17] E. van der Weide, H. Deconinck, E. Issmann and G. Degrez, Fluctuation Splitting Schemes for multidimensional convection problems: an alternative to finite volume and finite element methods, *Computational Mechanics*, Vol. 23, No. 2. pp: 199-208, 1999

[18] H. Deconinck, P.L. Roe and R. Struijs, A multidimensional generalization of Roe's flux difference splitter for the Euler equations, *Computers and Fluids*, Vol. 22, pp: 215-222, 1993

[19] C.W. Shu and S. Osher, Efficient Implementation of Essentially Non-oscillatory Shock Capturing Schemes, *Journal of Computational Physics*, Vol. 83, No. 1, pp: 32-78, 1989

[20] P. Colella and P. Woodward, *Journal of Computational Physics*, Vol. 54, pp: 115-173, 1984

[21] C.J. Hwang and J.L. Liu, Locally Implicit Hybrid Algorithm for Steady and Unsteady Viscous flows, *AIAA Journal*, 30:1228-1236, 1992